

The Effect of the Growth Condition on the Properties of the New Material $\text{Sn}_3\text{Sb}_2\text{S}_6$ Thin Films

A. Larbi^{1,*}, N. Khedmi¹ and M. Kanzari²

¹ Laboratoire de Photovoltaïques et Matériaux de Semi-conducteurs-ENIT-Universit de Tunis el Manar, BP 37, le belvédère1002-Tunis, Tunisie

² Laboratoire de Photovoltaïques et Matériaux de Semi-conducteurs-ENIT-IPEITunis Montfleury-Université de Tunis

Received: 7 Jun. 2012, Revised: 21 Sep. 2012, Accepted: 23 Sep. 2012

Published online: 1 Jan. 2014

Abstract: Sulfosalt $\text{Sn}_3\text{Sb}_2\text{S}_6$ material was synthesised by the horizontal Bridgman method. X-rays diffraction analysis of the powder showed that only homogenous $\text{Sn}_3\text{Sb}_2\text{S}_6$ phase is present in the ingot. $\text{Sn}_3\text{Sb}_2\text{S}_6$ thin films were deposited by a single source vacuum thermal evaporation with different thicknesses on glass substrates. The optical and structural properties of the films were studied as a function of thicknesses and temperature substrates. It is interest to note that $\text{Sn}_3\text{Sb}_2\text{S}_6$ films exhibit polycrystalline structures along (416) preferred plane without heating the substrates. In addition, we note that as the thickness increases from 150 nm to 430 nm the average grain size increases from 190 to 350 Å. The samples have direct bandgap energies of 1.5 - 1.75 eV. Furthermore, we found that the absorption coefficient in all cases reached 10^4 cm^{-1} . So, Sulfosalt $\text{Sn}_3\text{Sb}_2\text{S}_6$ thin films could be used as a potential candidate in may technological applications such as photovoltaic solar cells

Keywords: Sulfosalt, $\text{Sn}_3\text{Sb}_2\text{S}_6$, Thin films, Structural properties, Optical properties.

1 Introduction

The optical, structural and electrical properties of the sulfosalt materials have attracted great attention due to their interesting technological applications [1]. The objective of Scientifics is to obtain new materials which have in particular excellent optical and electrical properties. Therefore many researchers are working on different materials for achieving optimal properties [2, 3]. So a great effort to prepare thin films from novel semiconductor materials that contain only abundant and relatively less-toxic materials such as the sulfosalt system Sn-Sb-S is highly recommended. Pure and doped Sn-Sb-S sulfosalts thin films are careful as important for the use in many applications such solar energy conversion, electrical and optical thermo switching properties and other photoconductive applications [4, 5, 6, 7, 8]. In our laboratory we have already studied SnSb_2S_4 and $\text{Sn}_2\text{Sb}_2\text{S}_5$ thin films materials which showed interest physical properties such electrical and optical thermo switching [9, 10, 11, 12]. For that reason, this work deals with the study of another material of $\text{Sn}_x\text{Sb}_y\text{S}_z$ sulfosalt family that is the effect of thicknesses on the structural and optical

properties of the new absorber material $\text{Sn}_3\text{Sb}_2\text{S}_6$ in thin films forms.

2 Experimental Work

2.1 Synthesis of $\text{Sn}_3\text{Sb}_2\text{S}_6$

Stoichiometric amounts of the elements of 99.999 % purity Sn, Sb, and S were used to prepare the initial ingot of $\text{Sn}_3\text{Sb}_2\text{S}_6$. The mixture was sealed in vacuum in a quartz tube. We use the horizontal Bridgman method [13] to synthesize the material. In order to avoid explosions due to sulfur vapor pressure (2 atm to 493 °C and 10 atm to 640 °C), the quartz tube was heated slowly (20 °C/h) until 600 °C. A complete homogenization could be obtained by keeping the melt at 600 °C for about 48 h. The tube was then cooled at the rate 10 °C/h, so that cracking, due to thermal expansion of the melt on solidification, was avoided, after what we allow the tube to cool to room temperature. The compound obtained by this method has a gray color and ingot form (Figure 1). A crushed powder of this ingot was used as raw material for

* Corresponding author e-mail: larbiafef@yahoo.fr

the thermal evaporation. X-ray analysis of the powdered material (Figure 2) showed that only a homogenous $Sn_3Sb_2S_6$ phase was present in the ingot.

2.2 Film preparation

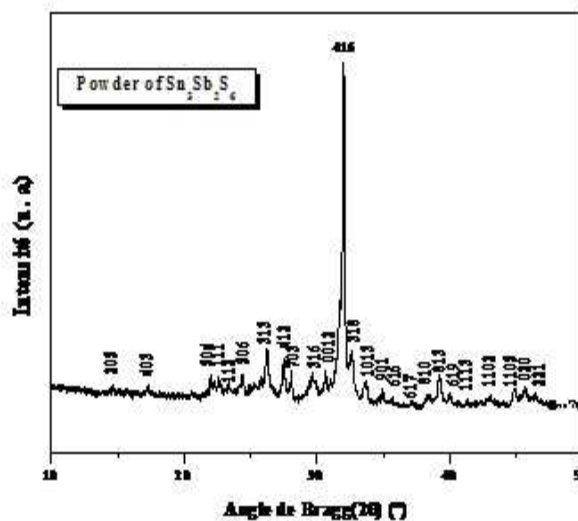
$Sn_3Sb_2S_6$ films for various thicknesses were deposited on glass substrates by single source thermal vacuum evaporation method. In the case of heated substrates the substrate temperature was taken 200 °C. The pressure during the evaporation was maintained at 10^{-5} Torr. A Chromel-Alumel thermocouple monitored the substrate temperature.

2.3 Characterization of the films

Structural properties were determined by X-ray diffraction (XRD) using $CuK\alpha$ radiation ($\lambda=1.54056 \text{ \AA}$). Optical transmittance and reflectance were measured at normal incidence with a UV-visible-NIR Shimadzu 3100S spectrophotometer in the wavelength range 300-1800 nm. The film thicknesses were calculated from the positions of the interference maxima and minima in the reflectance spectra using a standard method [14]. The film thicknesses were found to be in the range 150-430 nm.



Fig. 1: $Sn_3Sb_2S_6$ ingot



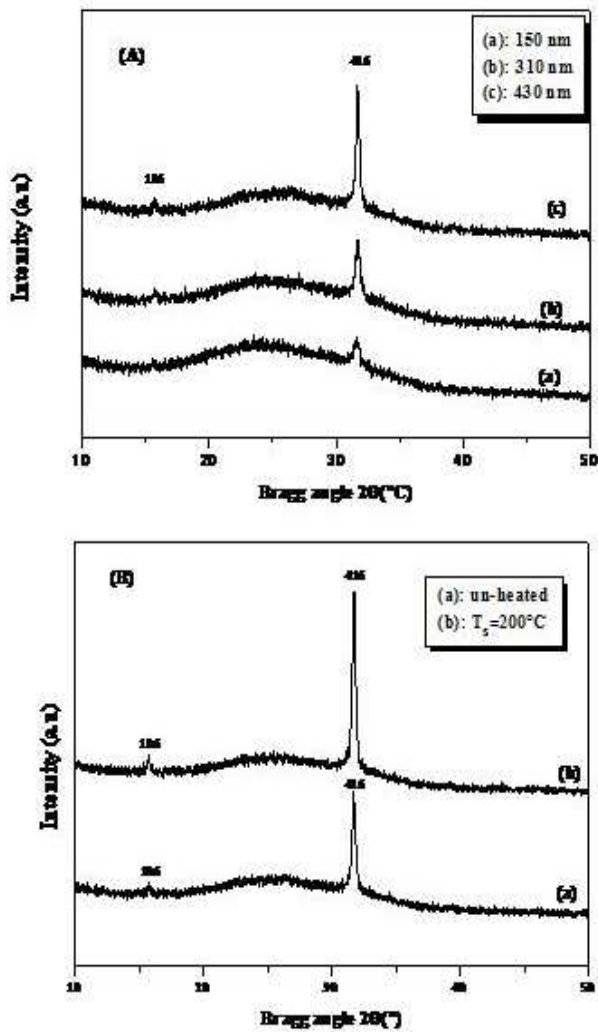


Fig. 3: X-ray diffraction patterns of $Sn_3Sb_2S_6$ thin films developed at different thicknesses (A) and at various substrate temperatures (B).

The appearance of interferences indicates a good homogeneity of the deposited films. It can be seen from figures 4 that the transmittance is affected by the thickness since the interferences increase by increasing the film thicknesses. On the other hand the reflectance decreases from 40 % to 20 % by increasing the film thickness from 150 nm to 430 nm respectively. The decrease of the transmittance and the reflectance values by increasing the thickness films is correlated to the change in structural properties. It is clear from figures 5 that the absorption edge moves to the strong wavelength when the substrate temperature increases from the room temperature to 200 °C.

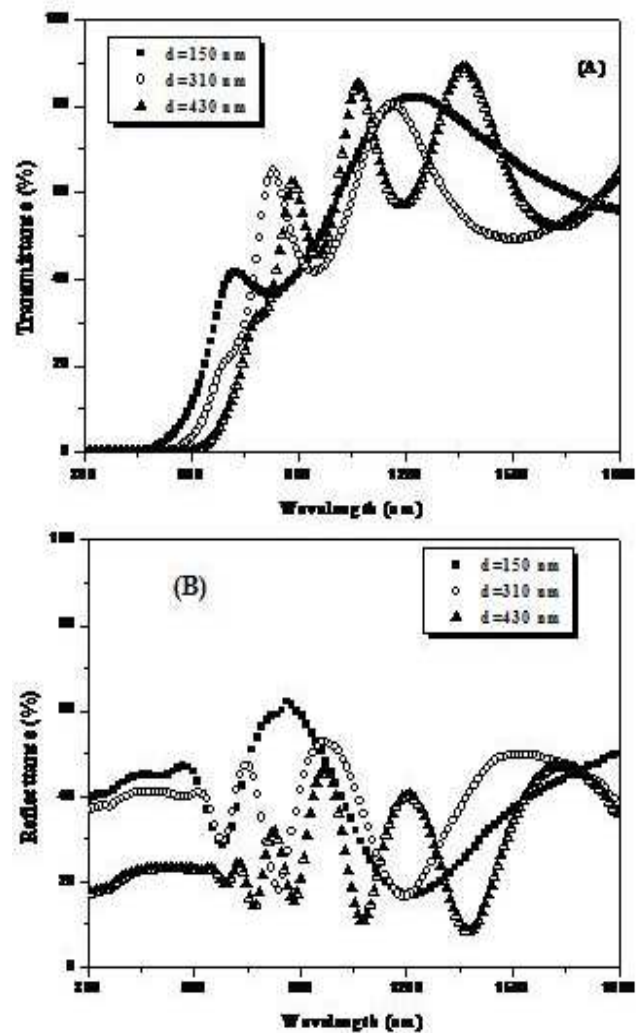


Fig. 4: Transmittance (A) and reflectance (B) spectra of $Sn_3Sb_2S_6$ thin films at various thicknesses

3.2.2 Absorption coefficients

The optical absorption coefficient α was evaluated from the transmittance (T) and reflectance (R) data by using the following formula [15]:

$$\alpha = \frac{1}{d} \times \ln\left(\frac{(1-R)^2}{T}\right) \quad (1)$$

Where α is the absorption coefficient and d is the film thickness. It is clear from figure 6 that α increases in the visible spectral range by increasing both the thickness and the substrate temperature. It can be seen also that the

$\text{Sn}_3\text{Sb}_2\text{S}_6$ films have relatively absorption coefficients, higher than 10^5cm^{-1} in the visible and the near-IR spectral region. This result is very important because it is known that the spectral dependence of the absorption coefficient is an important factor which affects the solar conversion efficiency.

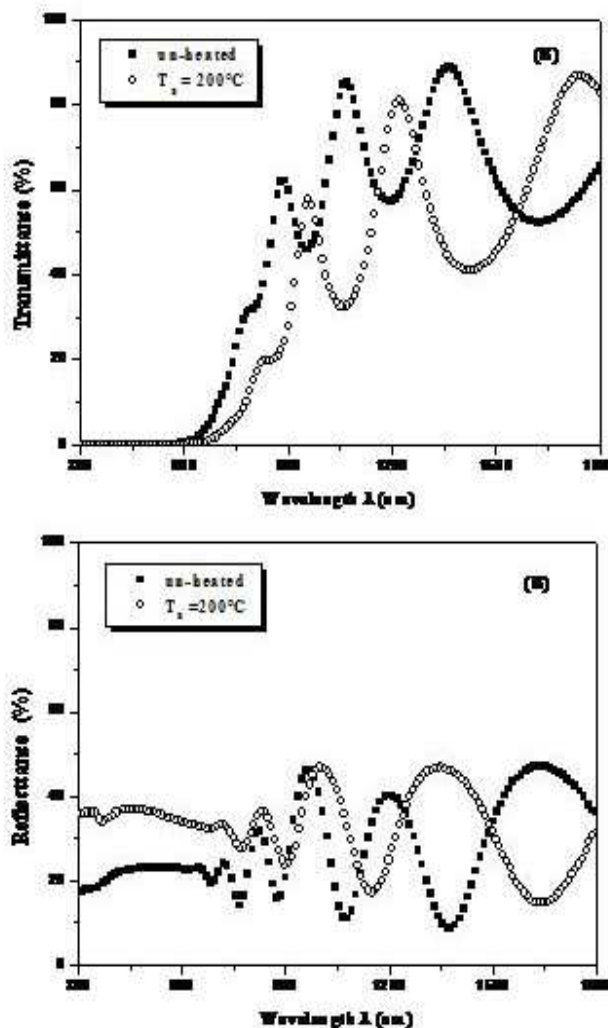


Fig. 5: Transmittance and reflectance spectra of $\text{Sn}_3\text{Sb}_2\text{S}_6$ thin films at various substrate temperatures.

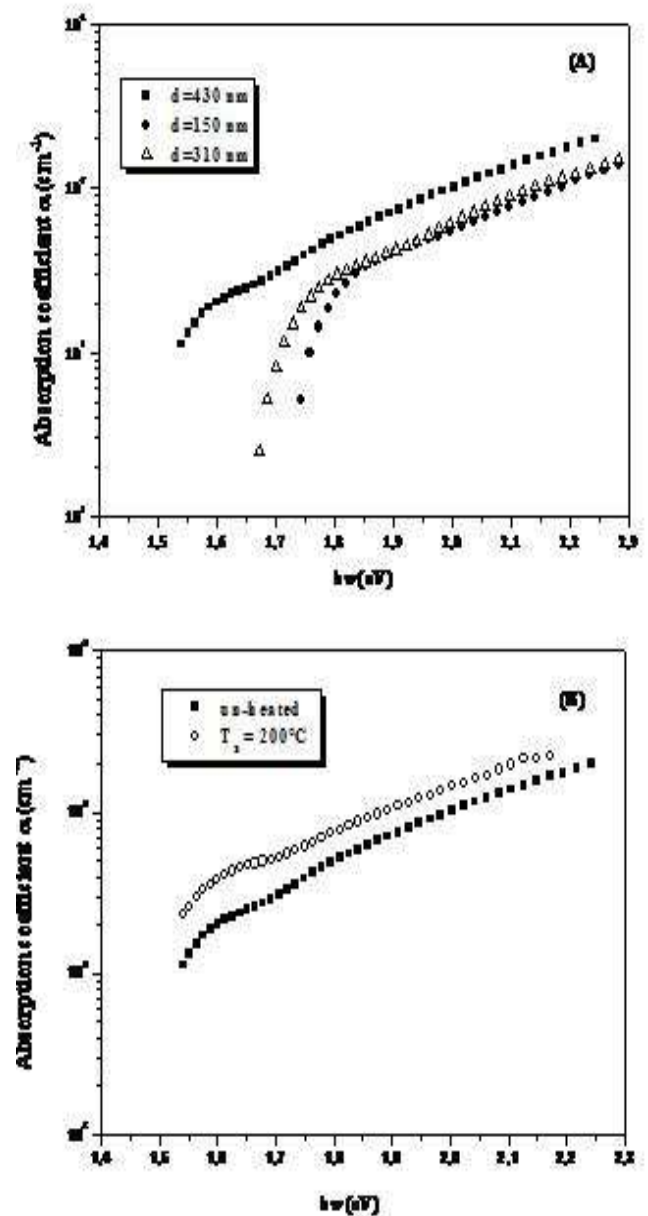


Fig. 6: Absorption coefficients of $\text{Sn}_3\text{Sb}_2\text{S}_6$ thin films at different thicknesses (A) and substrate temperatures (B).

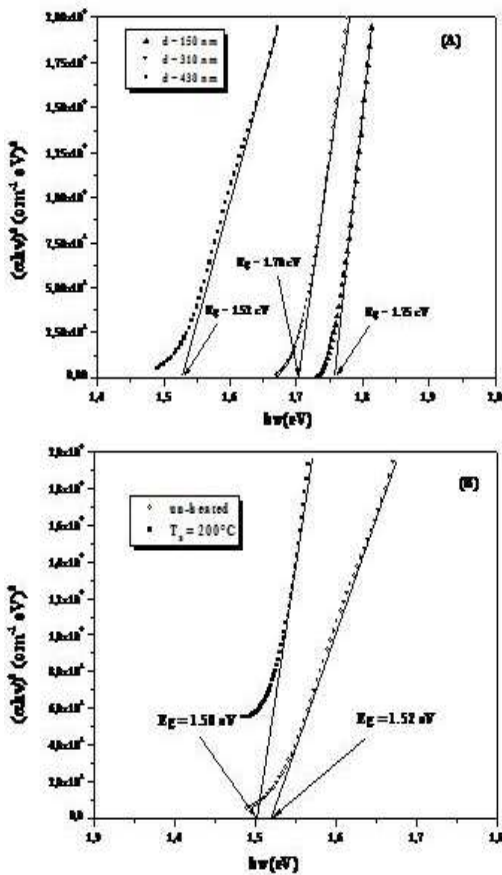


Fig. 7: Direct Band gap of $Sn_3Sb_2S_6$ thin films at different thicknesses (A) and substrate temperatures (B).

3.2.3 Energy gaps

The absorption coefficient α is related to the energy gap according to the equation [16]:

$$\alpha h\nu = A(h\nu - E_g)^n \quad (2)$$

Where A is a constant, h is the Planck constant and n is equal to 1/2 for a direct gap and 2 for an indirect gap. The band gap value E_g was determined by extrapolating the straight line of $(\alpha h\nu)^2$ versus $h\nu$ curve to the horizontal photon energy axis. Figure 7.A shows the behavior of $(\alpha h\nu)^2$ versus photon energy for the films. Two direct band gaps corresponding to the energy gaps E_{g1} and E_{g2} were found for thickness 310 and 430 nm. The energy gaps values are estimated to be in the range 1.75-1.70 eV for thickness 310 nm while for the thickness 430 nm, the energy gaps values are in the range 1.67-1.52 eV. The values correspond to the transition between the valence band and the conduction band. Concerning the low

thickness (150 nm) only a direct band gaps was observed and was near the values of 1.77 eV. The decrease of E_g may be attributed to the enhancement of grain size and the decrease of defects in microstructure, which give rise to defect states and thus induce a smearing out of the absorption edge. Figure 7.B shows the behavior of the gap energy E_g as a function of substrate temperature. It is clear that the value of the gap energy decrease from 1.55 eV to 1.49 eV by increasing the substrate temperature $200^\circ C$. These values are close to the theoretical optimum for efficient conversion of solar radiation into electrical power. The decrease in the values of the direct energy gap of $Sn_3Sb_2S_6$ thin films by increasing the substrate temperature could be attributed to several factors. Firstly, it may be attributed to the morphological change and the improvement of crystallinity affected by increasing the substrate temperature. Secondly, the stoichiometric deviations in the films which give rise to the formation of localized states in the band gap region.

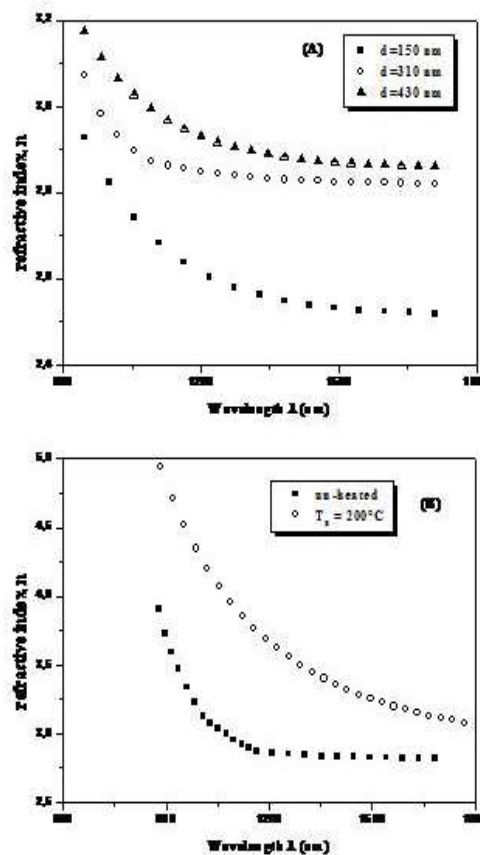


Fig. 8: Variation of refractive index n with wavelength for $Sn_3Sb_2S_6$ thin films at various thicknesses (A) and substrate temperatures (B).

3.2.4 Refractive index dispersion analyses

The values of the refractive indices (n) and extinction coefficients (k) of the $Sn_3Sb_2S_6$ films were calculated approximately from the method described in [17,18]. Figure 8 shows the refractive index, n , of the $Sn_3Sb_2S_6$ films as a function of wavelength for different thicknesses and substrate temperatures. The refractive index increases by increasing the thickness and substrate temperature confirming the increase of the opacity of the layers. So the opacity of the films is much correlated to the increasing of thickness and temperature. Figure 9 shows the extinction coefficient k of the $Sn_3Sb_2S_6$ thin films. It is obviously that the extinction coefficients appear to become important only in the spectral absorption region for wavelengths less than 800 nm. In the weak absorption region the relation between the refractive index n and the oscillator strength below the band gap is given by Wemple Didomenico [19].

$$n^2(h\nu) = 1 + \frac{E_d E_0}{E_0^2 - (h\nu)^2} \quad (3)$$

Where E_0 is the energy of the effective dispersion oscillator, E_d the so-called dispersion energy which measures the average strength of the interband optical transitions, and $h\nu$ the photon energy. Figure 10 shows the relation between $(n^2 - 1)^{-1}$ and the squared photon energy $(h\nu)^2$ for $Sn_3Sb_2S_6$ films. The values of E_d , E_0 and have been determined from the slope and the intersection of the straight lines with $(n^2 - 1)^{-1}$ axis. The different values of the oscillator parameters were summarized in the table 1. It was found that there exists a correspondence between E_d and E_0 , which can be expressed as $E_0 \simeq 2E_g$ [20]. For further analysis of the optical data, the dielectric constant is discussed according to the Spitzer-Fan model by [21].

$$\varepsilon_r = n^2 - k^2 = \varepsilon_\infty - \left(\frac{e^2}{\pi c^2}\right) \left(\frac{N}{m^*}\right) \lambda^2 \quad (4)$$

Where ε_∞ is the high-frequency dielectric constant in the absence of any contribution from free carriers, N/m^* is the carrier concentration to the effective mass ratio, is the electronic charge, and c is the velocity of light. Plotting ε_r versus λ^2 (Figure 11) and fitting to a straight line, the values of N/m^* and ε_∞ were estimated. It is significant to compare the values of ε_∞ obtained from the Wemple DiDomenico model (Figure 10) with those from the Spitzer-Fan model (Figure 11), they show satisfactory agreement. All the results determined from the models for the samples are summarized in the table 1.

4 Conclusions

Ingot of $Sn_3Sb_2S_6$ material was obtained by the horizontal Bridgman method. $Sn_3Sb_2S_6$ thin films with various

thicknesses were grown by vacuum thermal evaporation method on glass substrates (unheated and heated at 200 °C). Structural analysis of $Sn_3Sb_2S_6$ thin films revealed that the crystallinity increases by increasing the film thicknesses and substrate temperature and only the $Sn_3Sb_2S_6$ phase is present. The optical study has shown that these typical films have a good transmission. Strong absorption coefficients are in the range $10^5 \sim 10^6 \text{ cm}^{-1}$. Displacement of the absorption edge to lower energies with increasing the substrate temperature and the thickness causing the decrease of the band gap energies to the value 1.5 eV are observed. This value was a close to the theoretical optimum for efficient conversion of solar radiation into electrical power. Consequently, all the investigations properties give the new sulfosalt material a great importance in many technological applications such as thermoelectric energy conversion applications and thin film solar cells.

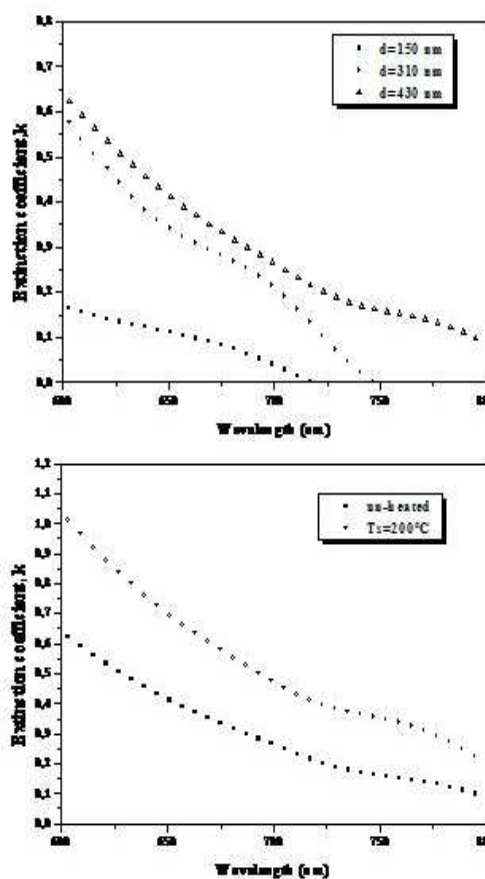


Fig. 9: Variation of extinction coefficient k with wavelength for $Sn_3Sb_2S_6$ thin films at various thicknesses and substrate temperatures.

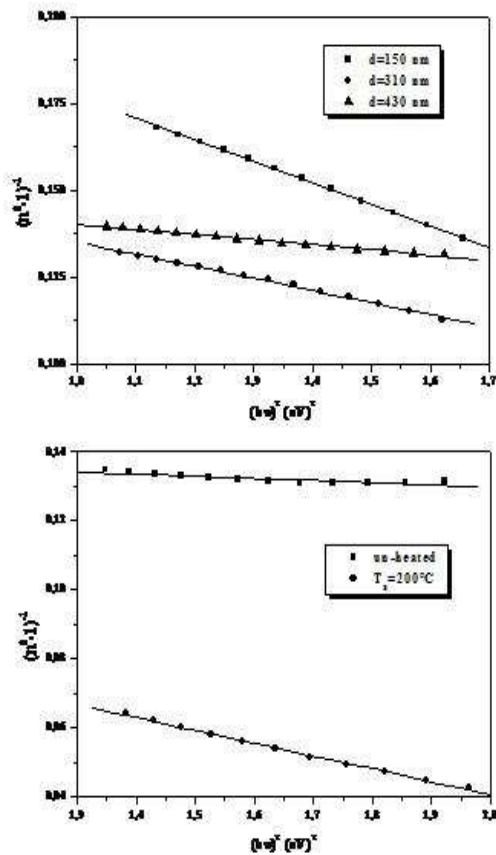


Fig. 10: Plot of $(n^2 - 1)^{-1}$ versus squared photon energy for $Sn_3Sb_2S_6$ thin films at various thicknesses and substrate temperatures.

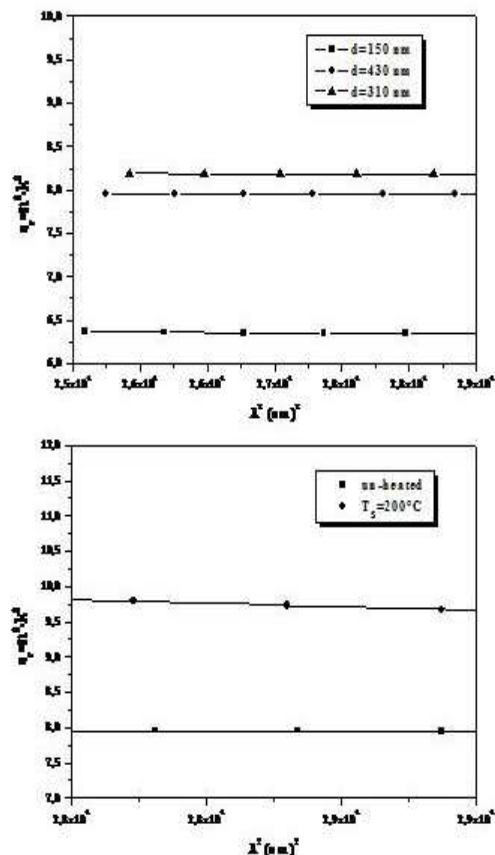


Fig. 11: Plot of optical dielectric constant versus wavelength squared for $Sn_3Sb_2S_6$ thin films at various thicknesses and substrate temperatures.

Table 1: The estimated values of optical parameters for $Sn_3Sb_2S_6$ thin film

t(nm)	T_s (°C)	E_0 (eV)	E_d (eV)	n(0)	E_g (eV)	E_0/E_g
150	30	03.03	09.90	02.32	01.75	01.73
310	30	02.99	13.83	02.57	01.70	01.75
430	30	03.25	20.65	02.73	01.52	02.13
	200	02.98	12.05	02.82	01.50	01.98

References

- [1] H. Dittrich, A. Bieniok, U. Brendel, M. Grodzicki, D. Topa, Thin Solid Films. 515 (2007) 5745.
- [2] Okoro OI, Madueme TC. International Journal of Sustainable Energy 25(1), 23 (2006).150.
- [3] Thirugnanasambandam M, Iniyana S, Goic R. Renewable and Sustainable Energy Reviews 14, 312 (2010).
- [4] K.Petkov, R. Todorov, D. Kozhuharova, L. Tichy, E. Cernoskova, P. J. S. Ewen.. J. Mat. Sci. 8, 39-96 (2004).
- [5] E. Marquez, A. M. Bernal-Oliva, J. M. Gonzales-Leal, R. Pietro-Alcon, T. Wagner. J. Phys. Appl. Phys. 39, 1793 (2006).
- [6] .Lu, H.Zeng, Z.Wang, X.Cao, L. Zhang. Nanotechnology 17, 2098 (2006).
- [7] Z.S.El Mandouh, S.N.Salama. Some physical properties of evaporated thin films of antimony trisulfide. J. Mat. Sci. 25, 1715 (1990).
- [8] AHMAD SAEED, NISAR ALI, WAQAR A. A. SYED, Chalcogenide Letters Vol. 10, No. 4, March 2013, p. 143 - 150.
- [9] A.Gassoumi, M. Kanzari and B. Rezig. Eur. Phys. J. Appl. Phys. 41, (2008) 91-95.
- [10] A.Gassoumi and M. Kanzari Journal of Optoelectronics and Advanced Materials, Vol.11 ISS4-(2009) 414 420.
- [11] A.Gassoumi, and M. Kanzari The Mediterranean Journal of Electronics and Communications, Vol. 5, No. 2, (2009) 66-72.
- [12] A.Gassoumi and M. Kanzari Physica E 44 (2011) 7174.
- [13] P. Rudolph, F. M. Kiessling, Crystal research and technology, 23 (1988).

- [14] M. Balkanski, T. S. Moss, Optical Properties of Semiconductors, Elsevier Science & Technology Books (1994).
- [15] M. Balkanski, T. S. Moss, Optical Properties of Semiconductors, Elsevier Science & Technology Books (1994).
- [16] E. A. Davis, N. F. Mott, Philipp. Mag. 22 (1970) 903.
- [17] M. Zribi, M. Kanzari , B. Rezig Materials Letters. 60 (2006) 98.
- [18] M. Caglar, S. Ilican, Y. Caglar, F. Yakuphanoglu, J. Mater. Sci.:Mater. Electron 19 (2008) 704.
- [19] S. Wemple, SH, Phys. Rev. B 7-8 (1973) 3767.
- [20] K. Tanaka, Thin Solid Films 66 (1980) 271.
- [21] B. Yous, J. M. Berger, J. P. Ferraton Eta. Donnadien, Thin Solid Films, 82 (1981) 279.